

COMPARATIVE ASSESSMENT OF PROPULSION SYSTEM ARCHITECTURES TAILORED FOR SUPERSONIC APPLICATIONS

Lorenzo Carrea[1] & Konstantinos Kyprianidis[1]

[1]Mälardalen University, Västerås, Sweden

Abstract

The return of economically and technologically sustainable civil supersonic transportation remains one of the most persistent challenges in modern aviation disciplines. Recent enhancements in materials, manufacturing processes, and engine technologies have renewed interest in the high-speed propulsion sector, with the aim of addressing both well-known longstanding and emerging limitations associated with the next-generation of supersonic travel.

Propulsion systems designed for sustained supersonic flight regimes must meet conflicting requirements, such as providing adequate enough thrust levels during specific portions of the mission, as well as maintaining efficient operation and performances comparable to the subsonic counterpart over the entire flight route.

In this context, Mixed Flow Turbofans targeting low-to-moderate bypass ratios and Variable Cycle Engines have emerged as suitable candidates due to their capabilities in delivering higher specific thrust than conventional unmixed turbofans.

In this study, the selected architectures are modelled and comparatively assessed using a Multi-Objective Optimization routine coupled with a Multi-Point Synthesis matching scheme engine design methodology. The design framework proposed enables the optimization of the main engine cycle design parameters, while enforcing propulsion system requirements and practical operational constraints across various critical key operating conditions. For each engine concept considered, a set of optimal candidate configurations is identified based on key performance indicators, fuel efficiency metrics, and preliminary weight estimates, and then compared with a previously benchmarked engine design.

The results show that the conventional configuration provides the most favourable mission installed SFC levels in the common objective space, while the variable cycle concept extends feasible design envelope toward substantially higher thrust dense regions and concurrently offering additional integration potential, at the cost of increased complexity, weight, and uncertainty.

Keywords: Supersonic Transport, Preliminary Engine Design, Mixed Flow Turbofan, Variable Cycle Engine, Multi-Objective Optimization

Abbreviations

AIP	Aerodynamic Interface Plane
BTR	Begin of Transonic Acceleration
CDF	Core Driven Fan
EI	Emission Index
ETR	End of Transonic Acceleration
FF	Front Fan
FMI	Functional Mock-Up Interface
FMU	Functional Mock-Up Unit
HPC	High-Pressure Compressor
HPT	High-Pressure Turbine
ICAO	International Civil Aviation Organization
JPL	Jet Propulsion Library
LPT	Low-Pressure Turbine
LTO	Landing and Take-Off
MFTF	Mixed Flow Turbofan
MOO	Multi-Objective Optimization
MPS	Multi-Point Synthesis
MTO	Maximum Take Off
NSGA-II	Non-dominated Sorting Genetic Algorithm II
OCT	Optimica Compiler Toolkit
RF	Rear Fan
SMCR	Supersonic Mid Cruise
SSBJ	Supersonic Business Jet
SST	Supersonic Transport
STOC	Supersonic Top of Climb

VABI	Variable Area Bypass Injector
VCE	Variable Cycle Engine
VGN	Variable Geometry Nozzle

Performance Metrics/Parameters

η	Efficiency	[%]
BPR	Bypass Ratio	[-]
FN	Net Thrust	[kN]
MPR	Mixer Pressure Ratio	[-]
OPR	Overall Pressure Ratio	[-]
PR	Pressure Ratio	[-]
SFC	Specific Fuel Consumption	[kg/N·s]
SFN	Specific Thrust	[m/s]

Superscripts and subscripts

bp	Bypass
c	Corrected
cr	Core
in	Inner
$inst$	Installed
out	Outer
ov	Overall
pol	Polytropic
$prop$	Propulsive
th	Thermal

1. Introduction

Although Concorde was retired from commercial service in 2003, the interest in civil supersonic aviation has not disappeared. On the contrary, the possibility of reducing long distance travel times continues to motivate research activities across academia, industry, and public institutions. Recent efforts aim to reassess the feasibility of Supersonic Transport (SST) in light of modern technologies, improved design approaches, stricter environmental expectations, and evolving certification and regulation standards [1].

The development of future SST aircraft is strongly connected to their environmental impact and societal acceptability. Compared with subsonic aviation, SST introduces additional challenges related to airport noise, pollutant emissions, climate impact, sonic boom, fuel consumption, and public acceptance [2, 3, 4]. These aspects are now central to the definition of future regulations and to the evaluation of whether civil supersonic operations can become commercially and environmentally sustainable. Within this context, several national and international initiatives have been launched to improve the understanding of the potential impact of future SST fleets, supporting the definition of suitable assessment methodologies. Among these initiatives, the European project SENECA [5] aimed on improving the understanding and modelling of SST related emissions, Landing and Take-Off (LTO) noise, and aircraft level global environmental impact, while providing more detailed assessment capabilities for the evaluation of future high-speed applications. Similarly, the MORE&LESS [6] project addressed the environmental sustainability of supersonic aviation through a multidisciplinary framework, considering different aircraft configurations, propulsion technologies, trajectories, and operations, while being compliant with environmental requirements.

Within this broader framework, the propulsion system design discipline remains one of the key enabler for future high-speed concepts. An engine capable of flying in supersonic regimes must satisfy requirements far more diverse and demanding than those encountered in conventional subsonic applications [7]. It has to provide sufficient thrust for high-speed cruise segments, operate reliably under more severe flight conditions, and maintain acceptable efficiencies across the entire mission. At the same time, the propulsion system should contribute to limit noise and emissions during LTO cycles and low altitude operations, while maintaining subsonic comparable fuel consumptions levels [8].

Within this context, Mixed Flow Turbofan (MFTF) architectures targeting low-to-moderate bypass ratios, together with Variable Cycle Engine (VCE) concepts, have been identified as promising solutions fro supersonic propulsion. These configurations can provide higher specific thrust than conventional unmixed turbofans, while avoiding severe fuel consumption penalties typically associated with traditional turbojet engines.

Among them, MFTF configurations represent a suitable reference architecture, given their favourable performance, reduced weight, and low risk and complexity, both for what concerns design and operation [9]. On the other hand, VCE architectures, represent an attractive candidate, given the increased and higher operational flexibility. By adapting the thermodynamic cycle through variable geometry components such as adjustable vanes, nozzles, and mixing systems, these propulsion system configurations can be tailored to different and conflicting performance requirements throughout the mission profile considered. This enables efficient subsonic operation while preserving the specific thrust required to maintain supersonic flight regimes during cruise [10]. The adoption of VCE con-

figurations leads therefore to a an engine design with fewer performance compromises compared to conventional "fixed-cycle" designs. These potential benefits are obtained at the expense of increased system level complexity. The additional degrees of freedom introduced by variable geometry components make the design, integration, and operation of the propulsion system more challenging.
Design choices at propulsion system level are strongly interconnected, and certain assumptions may improve performance metrics at a specific condition, while introducing penalties elsewhere in the mission. Therefore the assessment of a propulsion system designed to reach supersonic flight regimes should not be limited to isolated operating conditions, but it should instead account for the interactions among multiple mission segments and competing performance indicators.
A significant part of the available literature on civil supersonic propulsion focuses on specific aircraft classes and individual operating phases. Recent studies investigate Supersonic Business Jet (SSBJ) scale configurations, typically operating in the Supersonic Cruise Mach number range between 1.6 - 2.0 [11, 12, 13, 14], as well as larger airliner concepts with greater payload capacities, up to 300 passengers, and increased cruise Mach numbers [15, 16]. The focus is usually directed toward the identification of preliminary design trade-offs, LTO noise evaluation and mitigation procedures, emission estimations, and the effects of selected design variables on specific portions of the mission investigated [17, 18, 19, 20].
Although these studies provide valuable insights, a more comprehensive mission-level evaluation of the engine behaviour is still needed, to correctly assess supersonic cruise capability, off-design operation, fuel efficiency, LTO related constraints and engine practical operating limits, within the same framework.
The present work addresses this need by applying a Multi-Objective Optimization (MOO) procedure [21] to a Multi-Point Synthesis (MPS) matching scheme engine design methodology [22, 23]. The MPS approach enables simultaneous evaluation of on-design and multiple off-design operating conditions, while enforcing prescribed performance targets and engine limiters. The MOO routine is employed to explore the available design space and to identify possible main cycle design parameter combinations that provide suitable compromises between conflicting requirements [24]. The two engine architectures considered in this study (MFTF and VCE) are evaluated and assessed, and compared with a reference design.
Trade-off analyses are performed and a set of optimal configurations is selected for each engine architecture considering key performance indicators, cycle efficiency metrics and mass estimates. Aim of the study is to derive design guidelines and recommendations from the comparative assessment, relevant to the preliminary engine design process and specific for high-speed propulsion applications.

2. Methodology

The gas turbine engine models are developed using Modelon Impact, a Modelica-based simulation platform. Owing to the a-causal and object-oriented nature of the Modelica programming language, the resulting system of equations can be symbolically simplified, and the model construction can be carried out through reusable and hierarchical structures, while supporting system level modelling, simulation, and optimisation of complex energy systems [25]. Model development has been conducted using the Jet Propulsion Library (JPL) available in Modelon Impact, which offers pre-compiled and customizable components tailored to aero engine design disciplines, as well as built-in capabilities for on- and off- design simulations and for generating MPS matching schemes [26]. The final MPS models are compiled and exported as a Functional Mock-Up Unit (FMU) and executed within a Python environment via the Optimica Compiler Toolkit (OCT), respecting compliance with the requirements set by the Functional Mock-Up Interface (FMI) standard. This simulation setup and workflow enables interactions with external and third-party libraries, as well as established optimization packages.

2.1 Propulsion System Architectures

The engine architectures considered in this work are presented in Figure 1.
Both engine models include a supersonic intake component, to enable more accurate predictions of the propulsion systems' installed performance, critical in supersonic flight regimes. The intake

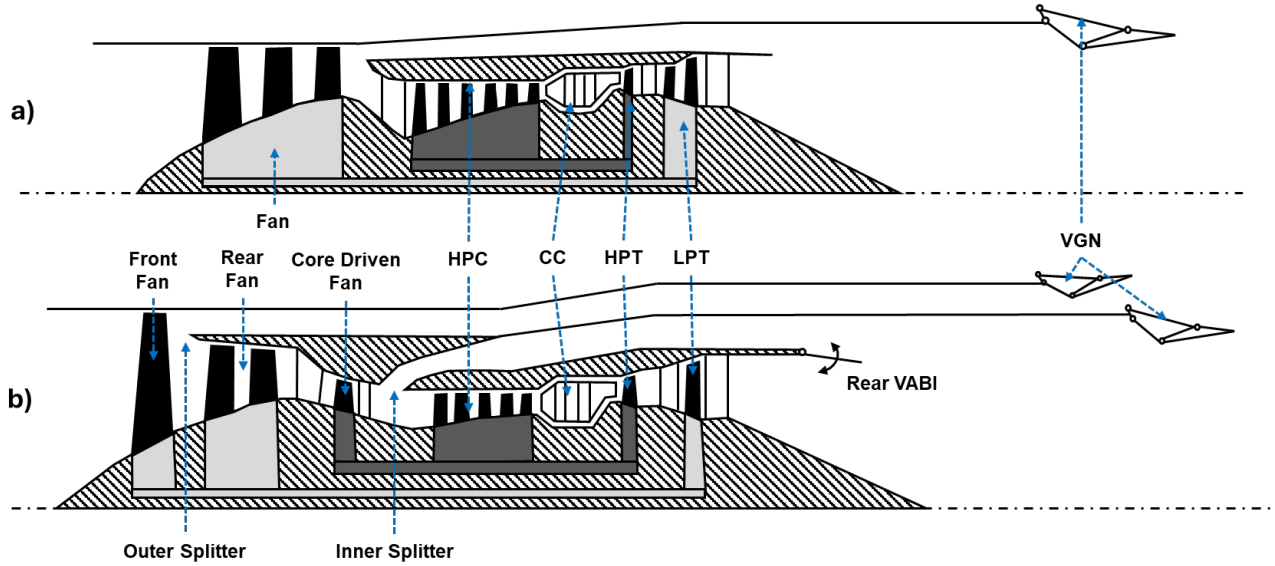


Figure 1 – Engine architectures considered: a) Mixed Flow Turbofan, b) Variable Cycle Engine

performance and component characteristics are based on the approach proposed in [27]. Pressure recovery factor, spillage drag coefficient, and other relevant intake parameters are provided as pre-tabulated datasets [28], as functions of the capture-to-freestream area ratio and flight Mach number, incorporating assumptions and operational constraints of the chosen intake component [29]. A bleed-less and bypass-less Normal Shock (NS) pitot inlet is selected given the design Mach number ($M = 1.5$), close to the speed regime considered in this study. Additional details regarding performance maps of the selected intake design are included in Figure 2. Thrust bookkeeping is performed accordingly, accounting for the additional drag components, while the effects of the intake shock system are captured by the pressure recovery factor at the engine inlet.

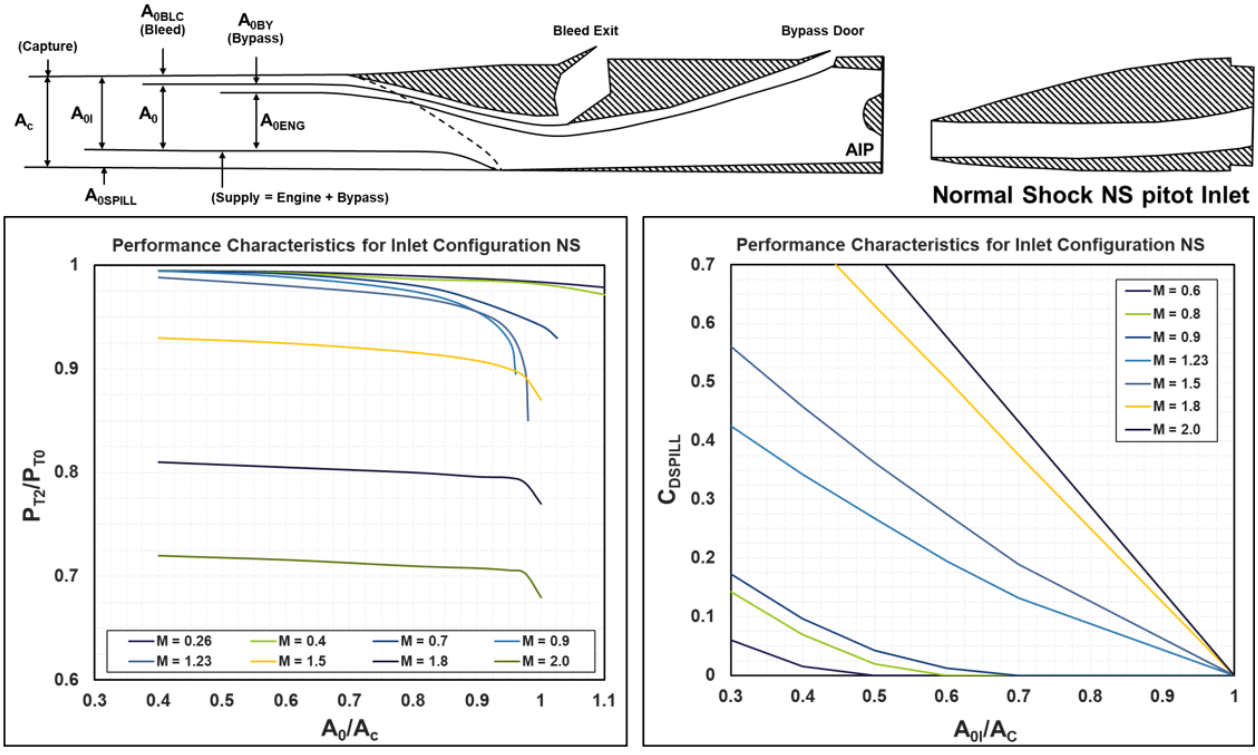


Figure 2 – Performance characteristics for the chosen intake design (NS)

Compressors located upstream of splitter components are modelled as radially split turbomachines,

following the methodology proposed in [30]. This approach accounts for the different core- and bypass-side characteristics along the blade span, while also capturing the mass flow distribution imposed by the position of the flow dividing streamline. Depending on splitter location with respect to the compressor outlet and off design variation of the BPR, different fractions of the inlet mass flow are partially compressed according to distinct characteristics before being mixed back into the respective ducts. In practice, the core- and bypass-side compressor characteristics are defined by assigning different PRs and polytropic efficiencies along the radial direction [31].
High-Pressure Turbine (HPT) and Low-Pressure Turbine (LPT) components have dedicated row-by-row secondary air system for nozzle guide vanes and rotor cooling. The cooling fractions required, defined as ratio of cooling mass flow to High-Pressure Compressor (HPC) inlet mass flow, are obtained by targeting either a maximum allowed uniform blade metal temperature or minimum cooling effectiveness, following the approach proposed in [32, 33]. The cooling fractions are defined in supersonic cruise operations, given the effect of ram compression, and differently from the subsonic counterparts which experiences the highest temperature levels during Take-Off phases.
Compressors and turbines performance modelling is conducted with in-house characteristic maps, which are scaled at the reference/design condition in the MPS matching scheme. Off-design behaviour is then modelled as outlined in [34].
The proposed engine architectures include Variable Geometry Nozzle (VGN). The variability of the nozzle throat area is introduced to provide additional noise reduction capabilities during low altitude operations and enhanced control features. The nozzle exit area is defined accounting for hardware limitations, in terms of maximum achievable area ratio. Therefore, at the nozzle outlet the expansion is not isentropic down to ambient pressure, but follows the empirical correlation based on measurement campaign proposed in [34]. Similarly as per the intake component, the same approach is used for the bookkeeping of nozzle-related installation effects [27]. Once again, for the chosen nozzle design, the underlying assumptions and performance characteristics are encapsulated into pre-tabulated datasets, enabling preliminary estimates of engine installed performance. The reference area used to calculate the aft-body drag coefficient is assumed to be 10 % larger than the nozzle exit area, obtained at the sizing reference condition.
No reheat system is considered, due to the environmental and noise related concerns extensively discussed by the authors in [24], and therefore not repeated here.

2.1.1 Mixed Flow Turbofan

As depicted in Figure 1 (a), the Fan component is driven by the LPT, the HPC is powered by the HPT, and they are respectively connected through low and high pressure shafts. The inlet flow is split at the Fan outlet and then mixed back at the LPT exit, before passing through the VGN.
The proposed layout represents a conventional architecture for supersonic propulsion and has been investigated in previous studies [24, 35].

2.1.2 Variable Cycle Engine

The proposed VCE configuration, shown in Figure 1 (b), consists of a LPT driven Fan component divided into Front Fan (FF) and Rear Fan (RF) blocks, a Core Driven Fan (CDF) connected to the high pressure shaft, and a conventional core (HPC and HPT). An outer splitter, located at the FF block exit, diverts part of the inlet mass flow to a co-annular third stream, which exits the engine through the bypass VGN. An inner splitter, located downstream the CDF block, bypasses a portion of the core mass flow, which is then reintroduced back in the core stream through a rear Variable Area Bypass Injector (VABI).
The decision to split the low pressure spool driven Fan is motivated by the additional capabilities offered by VCE architectures. The primary role of the third stream surrounding the engine core is to regulate and adjust the mass flow through the engine by means of the variable throat area of the bypass VGN. In addition to this, the third stream may provide heat-sink capabilities, offering further benefits from a system and sub-system integration perspective.

In view of possible future integration with electrical systems and more hybridized engine configurations, the availability of a dedicated flow path within the propulsion system may be advantageous. Electrical machines operating as motors, generators, or as intra-shaft power transfer enablers could introduce an additional degree of freedom in terms of flexibility, potentially reducing the need for variable geometries in the hot section of the engine. However, their integration would also introduce additional heat loads that would likely need to be dissipated within the propulsion system.
For the reasons above, the FF is assumed to adopt a single stage design, thereby limiting the maximum pressure ratio achievable, and therefore outlet temperature, enabling larger temperature gradients for potential heat rejection. Although the integration of a thermal management system or a more hybridized configuration falls outside the scope of the current study, these considerations were accounted for during the definition of the engine layout.
The rear VABI is modelled by enforcing conservation of the physical cross-sectional area and assuming static pressure balance between the two streams at the mixing plane. At the reference condition, the core and bypass inlet areas are sized by prescribing the core inlet Mach number (set to $\mathrm{Mach}_{\mathrm{cr,in}} = 0.5$). Based on these assumptions, the corresponding bypass stream Mach number is obtained. The resulting areas are then computed from the local flow conditions and define the cross section of the mixing area. A schematic of the component employed is depicted in Figure 3.
Under off-design conditions, the VABI mechanism modifies the ratio between the actual core area and the corresponding design value, defined as:

$$\alpha_{\mathrm{rear\,VABI}} = \frac{\mathrm{A_{cr,\,actual}}}{\mathrm{A_{cr,\,design}}},\ \text{with}\ (\alpha_{\mathrm{rear\,VABI}})_{\mathrm{design}} = 1 \tag{1}$$

Since the total mixer area remains constant, an increase in this ratio produces a reduction in the bypass flow area, while a decrease results in the opposite. The resulting variation in the core-to-bypass area ratio modifies the static pressure balance, affecting therefore the BPR in off-design operation.

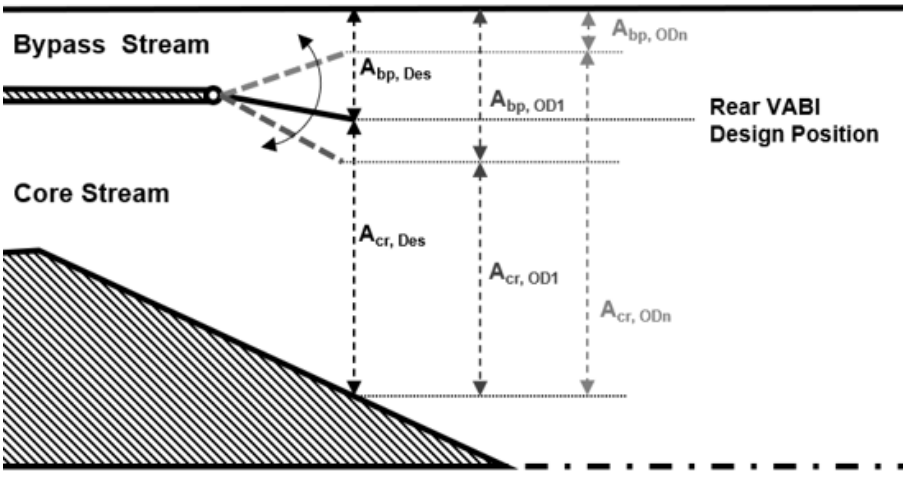


Figure 3 – Rear Variable Area Bypass Injector (VABI)

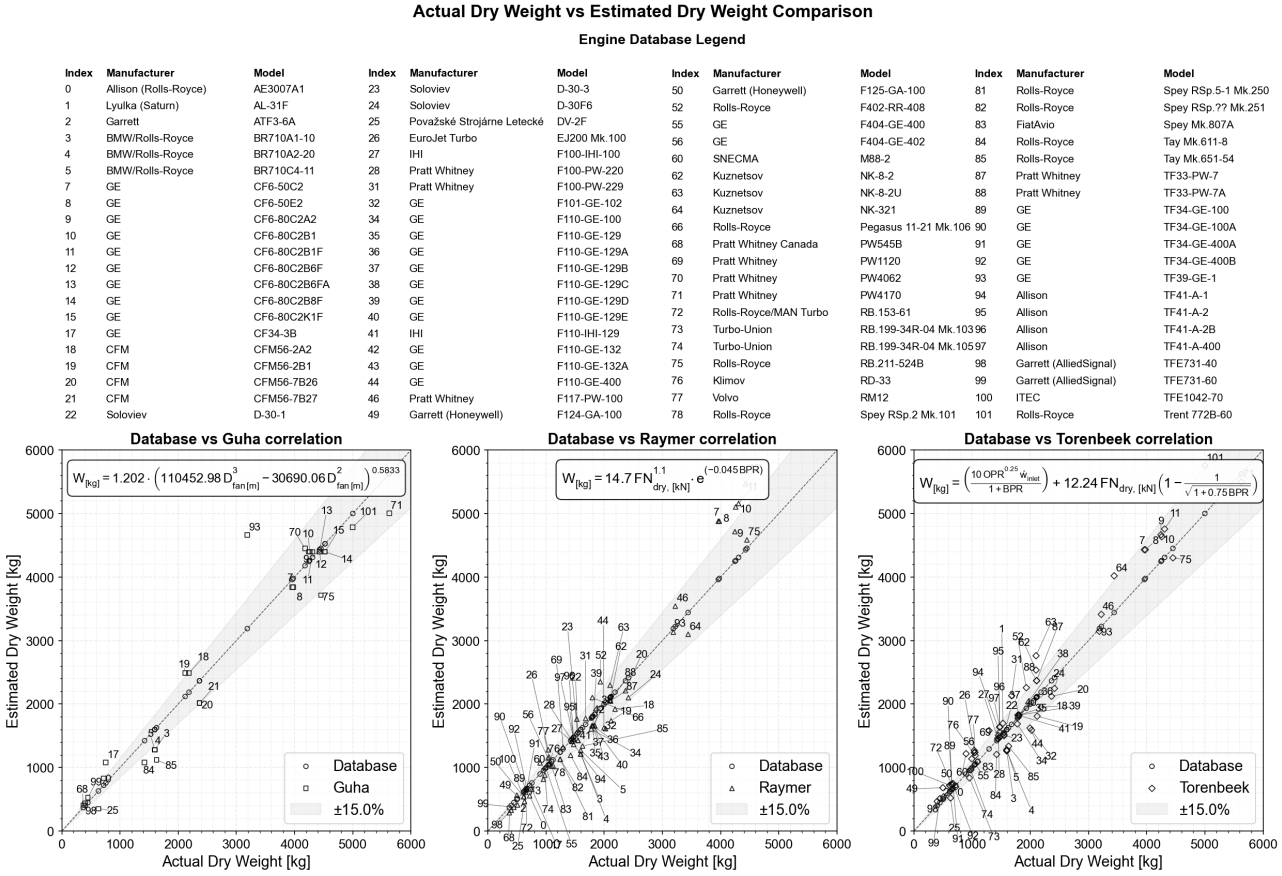
2.2 Emission Estimation

A preliminary estimation for pollutant emissions (CO_2, H_2O and NO_x) is performed for the operating conditions considered along the mission profile. The Emission Index (EI) for the NO_x species is obtained considering the semi-empirical correlation proposed in [36]. The correlation has been derived for modern RQL combustors using an extensive dataset of engine performance parameters and respective NO_x emissions measurement from the International Civil Aviation Organization (ICAO) databank. Given the good level of accuracy, it is considered suitable for application in the current study.

2.3 Preliminary Weight Estimation

A preliminary estimate of the propulsion system weight is performed using correlations available in public literature, which relate engine dry weight to one or more engine design parameters. Since the engine layouts considered fall within the class of low BPR MFTF and VCE configurations, a database of military engines was selected to compare the available weight estimation methods and to identify the most suitable.

Existing "whole engine based" preliminary weight estimates are summarised in [37, 38]. The correlations selected, and included in Figure 4, provide an increased level of detail by accounting for the interconnections between engine cycle design parameters and engine dry weight.



Index	Manufacturer	Model	Index	Manufacturer	Model	Index	Manufacturer	Model	Index	Manufacturer	Model
0	Allison (Rolls-Royce)	AE3007A1	23	Soloviev	D-30-3	50	Garrett (Honeywell)	F125-GA-100	81	Rolls-Royce	Spey RSp.5-1 Mk.250
1	Lyulka (Saturn)	AL-31F	24	Soloviev	D-30F6	52	Rolls-Royce	F402-RR-408	82	Rolls-Royce	Spey RSp.?? Mk.251
2	Garrett	ATF3-6A	25	Považské Strojárne Letecké	DV-2F	55	GE	F404-GE-400	83	FiatAvio	Spey Mk.807A
3	BMW/Rolls-Royce	BR710A1-10	26	EuroJet Turbo	EJ200 Mk.100	56	GE	F404-GE-402	84	Rolls-Royce	Tay Mk.611-8
4	BMW/Rolls-Royce	BR710A2-20	27	IHI	F100-IHI-100	60	SNECMA	M88-2	85	Rolls-Royce	Tay Mk.651-54
5	BMW/Rolls-Royce	BR710C4-11	28	Pratt Whitney	F100-PW-220	62	Kuznetsov	NK-8-2	87	Pratt Whitney	TF33-PW-7
7	GE	CF6-50C2	31	Pratt Whitney	F100-PW-229	63	Kuznetsov	NK-8-2U	88	Pratt Whitney	TF33-PW-7A
8	GE	CF6-50E2	32	GE	F101-GE-102	64	Kuznetsov	NK-321	89	GE	TF34-GE-100
9	GE	CF6-80C2A2	34	GE	F110-GE-100	66	Rolls-Royce	Pegasus 11-21 Mk.106	90	GE	TF34-GE-100A
10	GE	CF6-80C2B1	35	GE	F110-GE-129	68	Pratt Whitney Canada	PW545B	91	GE	TF34-GE-400A
11	GE	CF6-80C2B1F	36	GE	F110-GE-129A	69	Pratt Whitney	PW1120	92	GE	TF34-GE-400B
12	GE	CF6-80C2B6F	37	GE	F110-GE-129B	70	Pratt Whitney	PW4062	93	GE	TF39-GE-1
13	GE	CF6-80C2B6FA	38	GE	F110-GE-129C	71	Pratt Whitney	PW4170	94	Allison	TF41-A-1
14	GE	CF6-80C2B8F	39	GE	F110-GE-129D	72	Rolls-Royce/MAN Turbo	RB.153-61	95	Allison	TF41-A-2
15	GE	CF6-80C2K1F	40	GE	F110-GE-129E	73	Turbo-Union	RB.199-34R-04 Mk.103	96	Allison	TF41-A-2B
17	GE	CF34-3B	41	IHI	F110-IHI-129	74	Turbo-Union	RB.199-34R-04 Mk.105	97	Allison	TF41-A-400
18	CFM	CFM56-2A2	42	GE	F110-GE-132	75	Rolls-Royce	RB.211-524B	98	Garrett (AlliedSignal)	TFE731-40
19	CFM	CFM56-2B1	43	GE	F110-GE-132A	76	Klimov	RD-33	99	Garrett (AlliedSignal)	TFE731-60
20	CFM	CFM56-7B26	44	GE	F110-GE-400	77	Volvo	RM12	100	ITEC	TFE1042-70
21	CFM	CFM56-7B27	46	Pratt Whitney	F117-PW-100	78	Rolls-Royce	Spey RSp.2 Mk.101	101	Rolls-Royce	Trent 772B-60
22	Soloviev	D-30-1	49	Garrett (Honeywell)	F124-GA-100						

Figure 4 – Comparison between different preliminary weight estimation correlations against actual dry engine weight

Accounting for the expected dry weight range (between 1000 and 3000 kg), together with the availability of the required cycle design parameters, the correlation proposed by Torenbeek has been identified as the most appropriate for the analysis.

2.4 Propulsion System Design Strategy

The propulsion system design approach adopts the MPS matching scheme methodology, particularly suitable when conflicting requirements at different operating conditions must be taken into account. The method considered enables the simultaneous assessment of performance requirements, mission targets, and engine technological constraints, at selected operating points, assumed as critical corner conditions for propulsion system sizing and performance characterization [39, 40, 41].

Unlike the conventional iterative engine design process, the MPS approach allows multiple performance requirements to be evaluated concurrently, avoiding the need to sequentially adjust the design condition in order to satisfy off-design targets [42].

The left dashed box presented in Figure 5 summarizes the steps of the engine design strategy adopted.

2.5 Optimization Routine

The optimization framework is wrapped around the MPS matching scheme procedure, as shown in Figure 5, and it is designed to minimize or maximize competing performance metrics while assessing performance requirements and engine technical constraints at different operating conditions. The optimization strategy is based on Non-dominated Sorting Genetic Algorithm II (NSGA-II) [21].

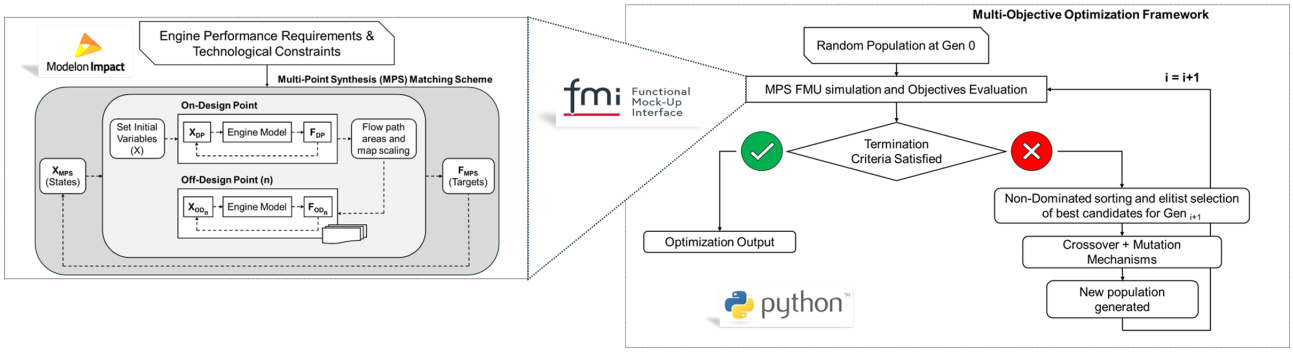


Figure 5 – Propulsion system design approach employed

NSGA-II is an elitist evolutionary algorithm that ranks candidate solutions into successive Pareto fronts according to dominance criteria. Within each front, the crowding distance is used to preserve diversity and prevent clustering in limited regions of the objective space, promoting in this way both convergence toward the optimal set of solutions while ensuring adequate distribution of suitable candidates along the optimal trade-off curve.

Starting from the initial population, in which each individual is generated by uniform sampling of the bounded decision variables, new generations are produced through elitist selection, simulated binary crossover and Gaussian mutation. The operators ensure recombination of suitable candidates while preserving diversity across the design space explored, ultimately yielding a Pareto-ranked population.

Each decision variable combination is supplied as input to the MPS model, and the objective variables are extracted and evaluated upon successful solver convergence. A warm-start strategy is used to initialize the iteration variables for each candidate evaluation: previously converged decision variable combinations are stored and compared in a normalized design space, and the closest available solution is selected for the initialization of iteration variables. The approach described provides the numerical solver a more informed and educated guess, improving robustness and reducing computational cost, without affecting the evolutionary mechanisms of the optimization algorithm.

The routine terminates when the Pareto front reaches a stagnation condition, while the maximum number of generations is retained as a safety cap. After a prescribed minimum number of generations, the current non-dominated front is compared with the historical Pareto archive. If no new or improved Pareto-optimal solution is identified for a prescribed number of consecutive generations, within the selected objective-space tolerance, the optimization is considered converged and terminated. Otherwise, the algorithm continues until the maximum number of generations is reached.

Some useful information related to NSGA-II are provided in Table 1.

2.5.1 Problem Formulation

The optimization is formulated as a multi-objective minimization problem. Each combination of the bounded decision variables reported in Table 2 (as main cycle design and off-design control parameters), is evaluated through the MPS matching scheme model across multiple mission point metrics. The independent objectives variables selected as optimization targets are represented by the $\mathrm{SFN}_{\mathrm{inst}}$ at the sizing condition and by a normalized weighted average of $\mathrm{SFC}_{\mathrm{inst}}$ across the multiple conditions considered. The optimization routine therefore searches for the Pareto set of non-dominated solutions in the multi-dimensional objective space.

Table 1 – Assumptions on main NSGA-II algorithm parameters

Parameter	Value
Population size	1000
Max generations	500
Termination Criteria	Pareto front stagnation
Stagnant generations before termination	5
Crossover factor	0.9
Crossover operator	Simulated binary crossover
Mutation factor	0.1
Mutation operator	Gaussian mutation
Random seed	40

Let $\mathbf{x} \in \mathbb{R}^n$ denote the vector of decision variables, and let $\mathbf{F}(\mathbf{x}) \in \mathbb{R}^m$ denote the vector of objective functions evaluated at the selected mission points in the MPS matching scheme. The optimization problem is stated as:

$$\min_{\mathbf{x}\in\Omega} \mathbf{F}(\mathbf{x}), \tag{2}$$

where Ω represents the bounded design space, and the vectors of decision variables (DV) and objective functions are defined as:

$$\mathbf{x} = [\mathrm{DV}_1, \mathrm{DV}_2, ..., \mathrm{DV}_\mathrm{n}], \tag{3}$$

$$\mathbf{F}(\mathbf{x}) = \begin{bmatrix} -\mathrm{SFN}_{\mathrm{inst,STOC}}(\mathbf{x}) \\ \mathrm{SFC}_{\mathrm{inst,mission}}(\mathbf{x}) \end{bmatrix} \tag{4}$$

The negative sign here is introduced for objectives that are maximized, since as mentioned above, the optimization routine is handled as minimization problem.
The normalized weighted installed specific fuel consumption is formulated as:

$$\mathrm{SFC}_{\mathrm{inst,mission}}(\mathbf{x}) = \sum_{k=1}^{N_{\mathrm{MP}}} w_k \cdot \mathrm{SFC}_{\mathrm{inst},k}(\mathbf{x}) \tag{5}$$

Here $\mathrm{N_{MP}}$ is the number of mission points included in the weighted metric, $\mathrm{w_k}$ is the weight associated with the $k-th$ operating condition, and $\mathrm{SFC}_{\mathrm{inst},k}$ is the corresponding $\mathrm{SFC_{inst}}$ evaluated at that condition.

Table 2 – Summary of the design/control parameters bounds adopted in the optimization setup

Design Parameter @ STOC	Unit	MFTF		VCE	
		min	max	min	max
$\dot{\mathrm{m}}_{\mathrm{inlet}}$	kg/s	50	90	50	90
T_{04}	K	1600	1950	1600	1950
$\mathrm{BPR}_{\mathrm{out}}$	-	-	-	0.05	0.15
$\mathrm{BPR}_{\mathrm{in}}$	-	0.3	1	0.15	1
$\mathrm{Fan}_{\mathrm{bp,PR}}$	-	3	5	-	-
$\mathrm{FF}_{\mathrm{bp,PR}}$	-	-	-	1.35	1.8
$\mathrm{RF}_{\mathrm{PR}}$	-	-	-	1.35	2.1
$\mathrm{CDF}_{\mathrm{bp,PR}}$	-	-	-	1.35	1.8
$\mathrm{HPC}_{\mathrm{PR}}$	-	5	11	5	11
Control Parameter @ Off-Design					
Nozzle $\mathrm{A}_{\mathrm{th,cr}}$ Scaling Factor	-	0.95	1.25	0.95	1.25
Nozzle $\mathrm{A}_{\mathrm{th,bp}}$ Scaling Factor	-	-	-	1	1.4
$\alpha_{\mathrm{rear\,VABI}}$	-	-	-	0.5	1.5

2.5.2 Constraints and Penalty Handling

The constraints included in the optimization are representative of engine aero thermodynamic practical limitations and performance requirements imposed in the MPS model, and they are summarized in Table 3. For each constraint, a normalized non-negative violation is computed as:

$$v_i(\mathbf{x}) = \begin{cases} \max\left(0, \dfrac{c_{i,\min} - c_i(\mathbf{x})}{c_{i,\min}}\right), & \text{for } c_i(\mathbf{x}) \leq c_{i,\min}, \\ \max\left(0, \dfrac{c_i(\mathbf{x}) - c_{i,\max}}{c_{i,\max}}\right), & \text{for } c_i(\mathbf{x}) \geq c_{i,\max}, \\ \dfrac{\left|c_i(\mathbf{x}) - c_{i,\text{target}}\right|}{c_{i,\text{target}}}, & \text{for } c_i(\mathbf{x}) = c_{i,\text{target}}. \end{cases} \tag{6}$$

where $g_i(\mathbf{x})$ is the value of the i-th constrained quantity, and $g_{i,\min}$, $g_{i,\max}$, and $g_{i,\text{target}}$ are the corresponding minimum, maximum, and target thresholds.
The total constraint violation of a candidate is then computed as follows:

$$V(\mathbf{x}) = \sum_{i=1}^{N_c} v_i(\mathbf{x}), \tag{7}$$

where N_c is the total number of active constraints. A candidate is considered feasible for the optimization if:

$$V(x) \leq \varepsilon_{\text{opt}}, \tag{8}$$

where ε_{opt} is the prescribed optimization feasibility tolerance. If a converged candidate violates the constraints beyond this tolerance, a penalty is applied to all transformed objective values supplied to the optimizer. The penalized objective vector is computed as:

$$\widetilde{F}^{\text{pen}}(\mathbf{x}) = \widetilde{F}(\mathbf{x}) + \lambda \left[\max\left(0, V(\mathbf{x}) - \varepsilon_{\text{opt}}\right)\right], \qquad V(\mathbf{x}) > \varepsilon_{\text{opt}}. \tag{9}$$

Here, $\widetilde{F}(x)$ is the objective vector after the sign transformation applied to maximization objectives, $\widetilde{F}^{\text{pen}}(x)$ is the penalized objective vector, and λ is the penalty coefficient.

Table 3 – Summary of active constraints considered in the optimization routine

Parameter	Value	Unit
$\text{FN}_{\text{inst,STOC}}$	$\geq$ Req. from Table 4	kN
$\text{FN}_{\text{inst,off-design}}$	$=$ Req. from Table 4	kN
$\text{Fan Diameter}_{\text{AIP}}$	≤ 1.2	m
$\text{Mixer inlet Mach}_{\text{bp,cr}}$	$0.1 \leq x \leq 0.8$	-
Compressors Surge and Choke Margin	$10 \leq x \leq 45$	%

2.6 Case Study Description

In this work, a 10 passengers SSBJ for a typical transatlantic mission (roughly 4000 nm) [43] is chosen as case study. The mission key corner points considered in the MPS matching scheme are namely Supersonic Top of Climb (STOC) (considered a reference operating condition), Supersonic Mid Cruise (SMCR), Maximum Take Off (MTO), Begin of Transonic Acceleration (BTR), and End of Transonic Acceleration (ETR). More details related to the operating conditions and the thrust requirements are included in Table 4.
The engine technology levels, assumed for a current entry into service year (2020), are based on supersonic engine design public domain [15, 44, 45], and have been corrected accordingly considering the potential improvements achievable in a future entry into service year (2040). Increases of 5K/year and 3K/year have been considered in maximum allowed gas and material temperature, following the trends proposed in [46].

Table 4 – Engine Performance Requirements from [44]

Operating Point	Altitude [m]	Flight Mach [-]	$\mathrm{FN_{inst}}$ Requirement [kN]
STOC (Ref.)	14800	1.6	25.8
SMCR	16300	1.6	18.2
MTO	0	0.3	67.9
BTR	10000	0.95	27.6
ETR	10000	1.3	38.3

The radially split compressors are modelled considering a fixed ratio between core and bypass section, aiming to fan blade design with constant span-wise work distribution [20], as formulated below:

$$\mathrm{PR_{cr}} = \mathrm{PR_{bp}} * 0.8875 \tag{10}$$

In Table 5 are summarized the main assumption and corrections on the engine technology levels, in the form of turbomachineries polytropic efficiencies and engine limiters. It should be noted that for low altitude operating conditions, (i.e. MTO) a higher temperature threshold is permitted ($\Delta T = +100\,K$).

Table 5 – Main assumptions on engine technology levels considered

Parameter	Configuration	EIS2020	EIS2040	Unit
$\mathrm{Fan_{bp}}$, $\mathrm{Fan_{cr}}$ η_{poly}	MFTF	Datum	+1	%
$\mathrm{FF_{bp}}$, $\mathrm{FF_{cr}}$ η_{poly}	VCE	Datum	+1	%
RF η_{poly}	VCE	Datum	+1	%
$\mathrm{CDF_{bp}}$, $\mathrm{CDF_{cr}}$ η_{poly}	VCE	Datum	+1	%
HPC, HPT, LPT η_{poly}	Both	Datum	+0.5	%
HPT, LPT $\mathrm{TBU_{max}}$	Both	Datum	+60	K
$\mathrm{T_{03\,max}}$, $\mathrm{T_{04\,max}}$	Both	Datum	+100	K
LP & HP Shafts $\mathrm{N/N_{ref}}$	Both	1.03	1.03	-
LP & HP Shafts $\mathrm{N_c/N_{c\,ref}}$	Both	1.0	1.0	-

The engine is sized at the reference condition adopted in the MPS matching scheme (STOC). The inlet mass flow is allowed to vary within the prescribed range, as reported in Table . The thrust requirement at STOC is imposed only as a lower bound, and therefore higher installed thrust levels are permitted at the reference condition, as long as the other performance requirement in off-design operations are satisfied. As a consequence, the adopted approach allows engine over-sizing at the design condition.

3. Results and Discussions

The results obtained from the MOO routine are presented in the following sections. Each engine architecture is compared against its corresponding reference design (sections 3.1 and 3.2), and candidate designs belonging to the best set of non-dominated solutions are selected. Then, in Section 3.3 a cross-comparison is performed to highlight the potential benefit and limitations of each engine architecture.

For both configurations, several assumptions were introduced in the definition of the reference design. Each baseline was defined by matching the installed thrust requirements reported in Table 4 and by targeting the same installed specific thrust level at design condition (STOC). This was achieved by varying the bypass Fan PR for the MFTF configuration and the RF PR for the VCE architecture. This choice allowed the two propulsion system layouts to retain the same engine size in terms of inlet mass flow, and therefore, given the same operating condition, fan diameter. The same HPC outlet temperature was imposed by adjusting the corresponding PR, while same combustor outlet temperature levels have been maintained at STOC. The SMCR mixer PR has been set to unity by adjusting

the bypass ratio of the corresponding bypass system. These assumptions were introduced at the preliminary stage to establish a consistent basis for comparison between the selected architectures.

3.1 Mixed Flow Turbofan

The MFTF configuration is first assessed in the objective space defined by the variation of the installed specific thrust at the MPS scheme sizing condition and the mission weighted installed specific fuel consumption, both evaluated with respect to the baseline configuration. The optimization outcomes, reported in Figure 6, indicate that performance improvements are available in both objective directions.

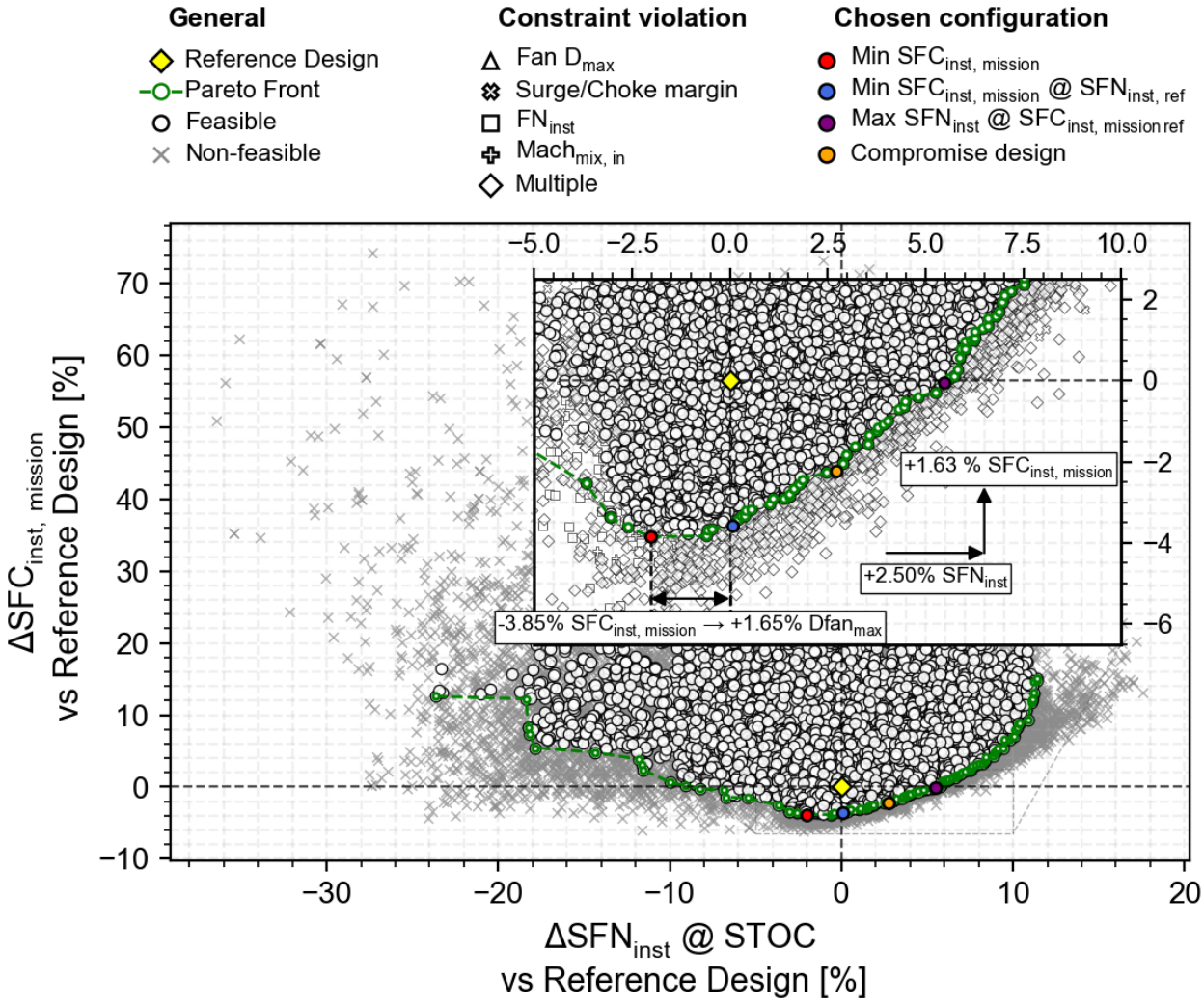


Figure 6 – Objective space trade-off for MFTF architecture, expressed as percentage variation relative to the reference design. Feasible and non feasible solutions are shown, with the set of non dominated solutions and selected suitable candidates

By appropriately tuning the design and control variables, while maintaining mission fuel consumption close to the baseline level, the installed specific thrust can be increased by almost 5.1%. This may be interpreted either as an additional thrust margin at approximately constant engine size, potentially allowing the engine to operate at lower power settings, or as an opportunity to reduce engine size while preserving the required thrust level. These two interpretations have different implications across the operating envelope. A larger thrust margin could also broaden the applicability of the engine while retaining similar dimensions, potentially enabling its use across aircraft of different sizes or thrust requirements. Conversely, a reduction in engine size could be beneficial when accounting for propulsion system weight and aircraft-level integration aspects.

At fixed engine size, and therefore at approximately constant installed specific thrust, the mission installed specific fuel consumption can be reduced by almost 3.8% without incurring in potential penalties associated with an increase in fan diameter. The overall minimum installed SFC is instead obtained by accepting a reduction in installed specific thrust, implying an enlargement of the Fan diameter. This behaviour can be associated with the improvement in propulsive efficiency, which has a favourable effect on the overall propulsion system performance. Within the region of interest of the objective space, a compromise solution can be selected, enabling a moderate reduction in mission installed SFC, while providing a slight increase in installed specific thrust.
The selected MFTF candidates should therefore be interpreted as representative design intents rather than isolated optimum points. The minimum installed SFC candidate identifies the most fuel efficient solution within the explored trade-off, while the candidate selected at reference installed specific thrust quantifies the SFC reduction achievable without decreasing the baseline dimensions. Conversely, the maximum installed specific thrust candidate represents the opposite side of the trade-off, where thrust capability is prioritized while maintaining mission SFC close to the reference value. The compromise design lies between these extremes and provides a balanced candidate for the subsequent cross-comparison with the VCE architecture.

3.2 Variable Cycle Engine

The VCE configuration is also assessed in the same objective space adopted for the MFTF. In this case, the results are expressed as percentage referred to the VCE baseline reference condition. As reported in Figure 7, the variable presents a wider feasible design space, with respect to the architecture baseline, with the Pareto front extending toward both reduced installed specific fuel consumption and substantially increased installed specific thrust.
At approximately constant installed specific thrust, the VCE architecture allows a reduction in mission installed SFC of about 7% relative to its own baseline. This indicates that the architecture can provide a relevant improvement in fuel consumption without necessarily reducing the reference size. On the other hand, when the optimization prioritizes installed specific thrust, improvements above 15% can be achieved while maintaining mission installed SFC close to the VCE reference value. This highlights one of the expected advantages of the variable cycle concept, namely its ability to adapt the cycle in order to support higher specific thrust requirements when needed.
The minimum SFC candidate is located on the low side of the Pareto front and is associated with a substantial reduction in mission installed SFC, but also with an increase in fan diameter. Therefore, as for the MFTF case, part of the fuel consumption benefit is obtained by moving toward a larger propulsion system. Within the selected region of interest, the local trade-off shows that an increase of 2.5% in installed specific thrust requires an increase of approximately 1.3% in mission weighted installed SFC. Compared with the corresponding MFTF exchange rate, where the same installed specific thrust increase is associated with a SFC penalty of about 1.6%, the VCE configuration exhibits a more favourable local objective space trade-off when each architecture is evaluated relatively to its own baseline.
This result is consistent with the expected behaviour of a variable cycle engine, which is designed to increase operating flexibility by enabling both high specific thrust operation and improved fuel consumption at lower power settings. However, the operating conditions considered in the present analysis do not fully exploit the low power setting capability of the architecture. More specifically, STOC, SMCR, and ETR points require operation in supersonic regime and are therefore representative of high thrust settings and at almost full throttle conditions, while the remaining operating points are not representative of low power operation. Consequently, the benefits observed here should be interpreted primarily as high power cycle matching and thrust flexibility effects, rather than as a complete assessment of the low power fuel saving potential of the VCE architecture.
The selected VCE candidates therefore represent the same design intents adopted for the MFTF analysis, but evaluated with respect to the VCE reference configuration.

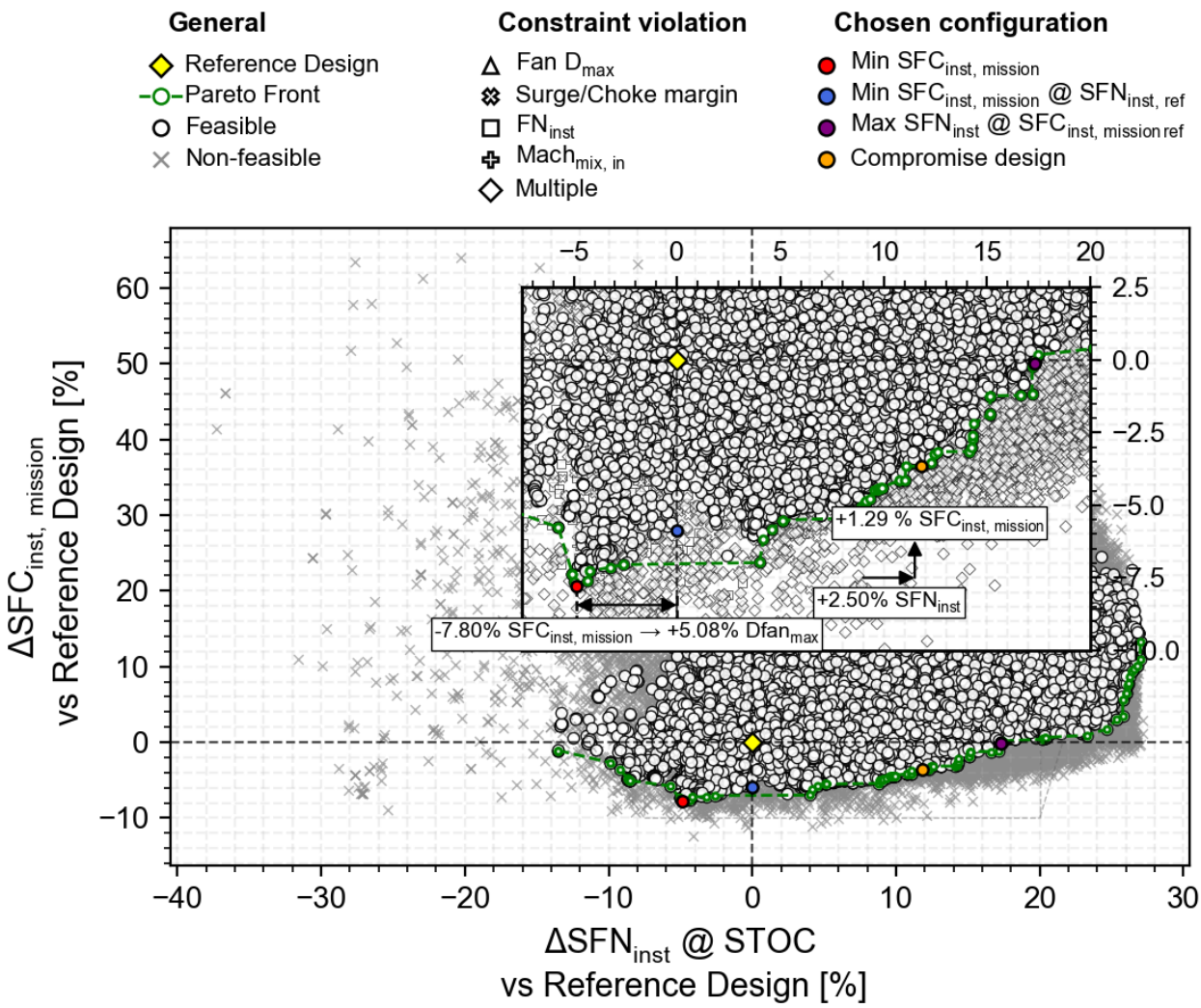


Figure 7 – Objective space trade-off for VCE architecture, expressed as percentage variation relative to the reference design. Feasible and non feasible solutions are shown, with the set of non dominated solutions and selected suitable candidates

3.3 Comparative Assessment

The two architectures are compared in a common objective space, as presented in Figure 8, where all variations are expressed with respect to the VCE baseline configuration. This choice enables the evaluation of configuration specific Pareto fronts, reference designs, and landmark candidates on a consistent basis. The comparison shows that the two architectures offer different design opportunities. The MFTF configuration is generally more favourable in the low-to-moderate specific thrust region, where it provides lower mission level installed SFC values than the VCE baseline. As notable from the figure below, the reference MFTF design lies already in a more appealing condition when looking at the installed SFC before even considering optimized solutions. This can be attributed to the conventional architecture itself, under the assumptions adopted for the baseline definition: fewer components contribute to the overall propulsion system losses, and the absence of an additional bypass nozzle avoids part of the thrust bookkeeping penalties associated with the installation effects within the VCE layout.

The VCE architecture, on the other hand, extends both the feasible region and the Pareto front toward significantly higher installed specific thrust regions. This highlights one of the main advantages of the advanced architecture: the capability to provide larger thrust density levels, while maintaining mission installed SFC within a comparable range.Therefore, the VCE does not necessarily appears as the most fuel efficient solution across the whole objective space, but it offers a wider operating flexibility in high specific thrust requirements.

This distinction is fundamental for the interpretation of the selected candidates. The conventional configuration primarily provides fuel consumption oriented improvements, while the adaptive configuration captures also the capability of delivering increased thrust levels without incurring in unacceptable SFC penalties. When considering the local trade-off in the region of interest, the same installed specific thrust increase is associated with a milder SFC penalty for the VCE case. However, the MFTF non dominated set remains shifted toward lower installed SFC levels, for most of the investigated region. The main benefit obtained from the variable cycle concept, is therefore not necessarily to an absolute mission installed SFC potential reduction, but rather the possibility of increasing the specific thrust levels, while limiting the associated performance deterioration due to fuel consumption penalties.

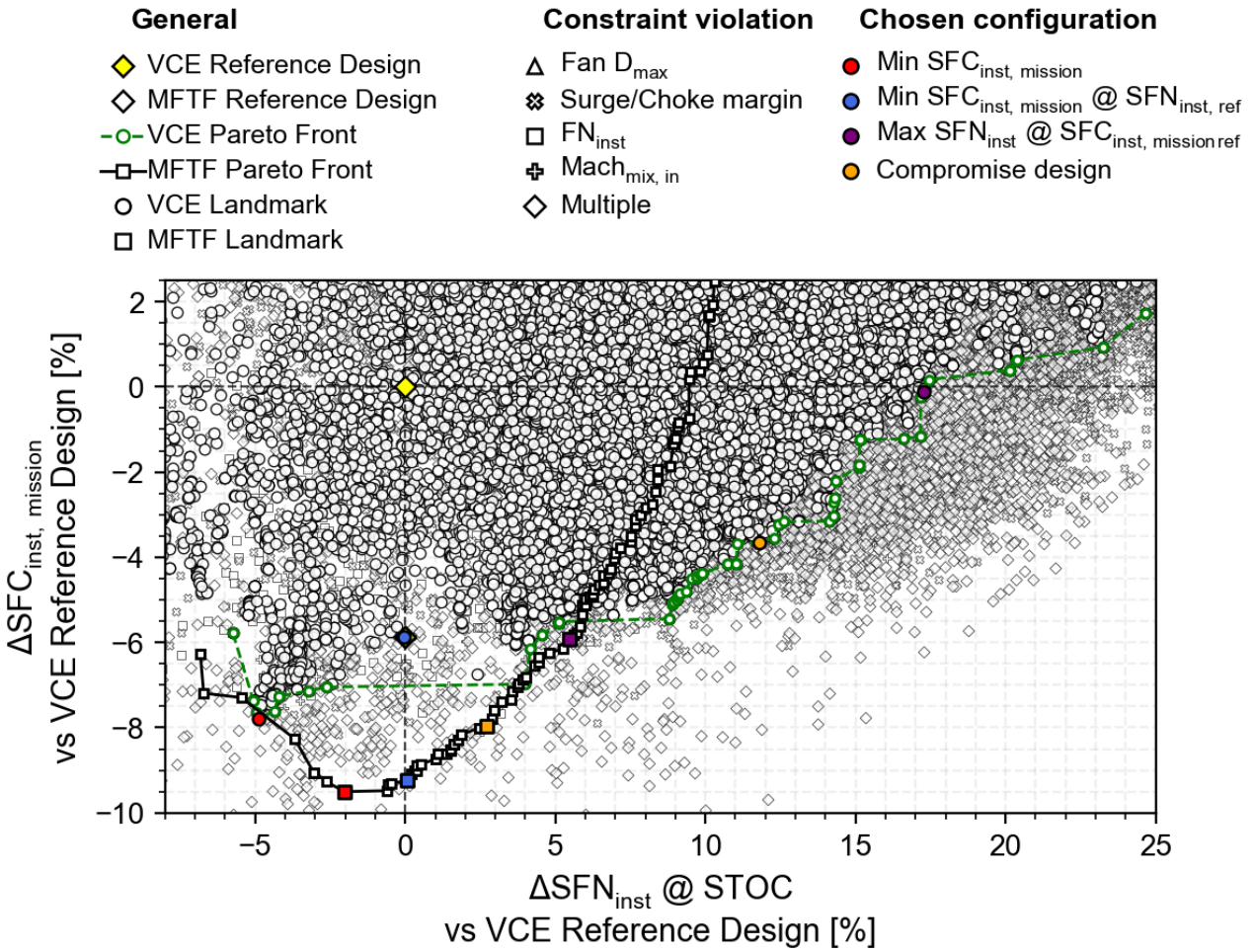


Figure 8 – Comparison of the MFTF and VCE trade-offs, expressed with respect to VCE reference design

Further insights on the potential improvements of thrust density levels enabled by the advanced architecture are provided in Figure 9. The figure reports the same shared objective space, again expressed relative to the VCE baseline configuration, but focus the attention on each architecture separately. In the upper row, the feasible point collection is coloured according to the variation in Fan diameter, while the lower row reports the corresponding variation in installed thrust. This representation helps to distinguish whether changes in installed specific thrust are mainly driven by variations in engine size or by changes in delivered installed thrust. For the MFTF configuration, the feasible region is associated with relatively moderate variations in both Fan diameter and installed thrust. On the other hand, the VCE architecture allows substantially larger increases in installed thrust, leading to higher installed specific thrust levels, with variations approximately in the range of 10 to almost 20% in the explored region. These improvements are achieved without prohibitive penalties in mission

installed SFC, highlighting once again the potential of the VCE architecture to extend the installed specific thrust envelope beyond the one of conventional configurations.
The potential benefits of VCE architectures should also be interpreted in light of its intended operational flexibility. Advanced cycle configurations are expected to provide benefits both in high specific thrust operation, as well as in lower power settings condition, where a more fuel efficiency behaviour is required. The full assessment of the potential benefits and drawbacks for these kind of configurations may be biased by the assumptions taken in the current study, and a more dedicated analysis on scheduling of variable geometries would close the assessment from a propulsion system level.

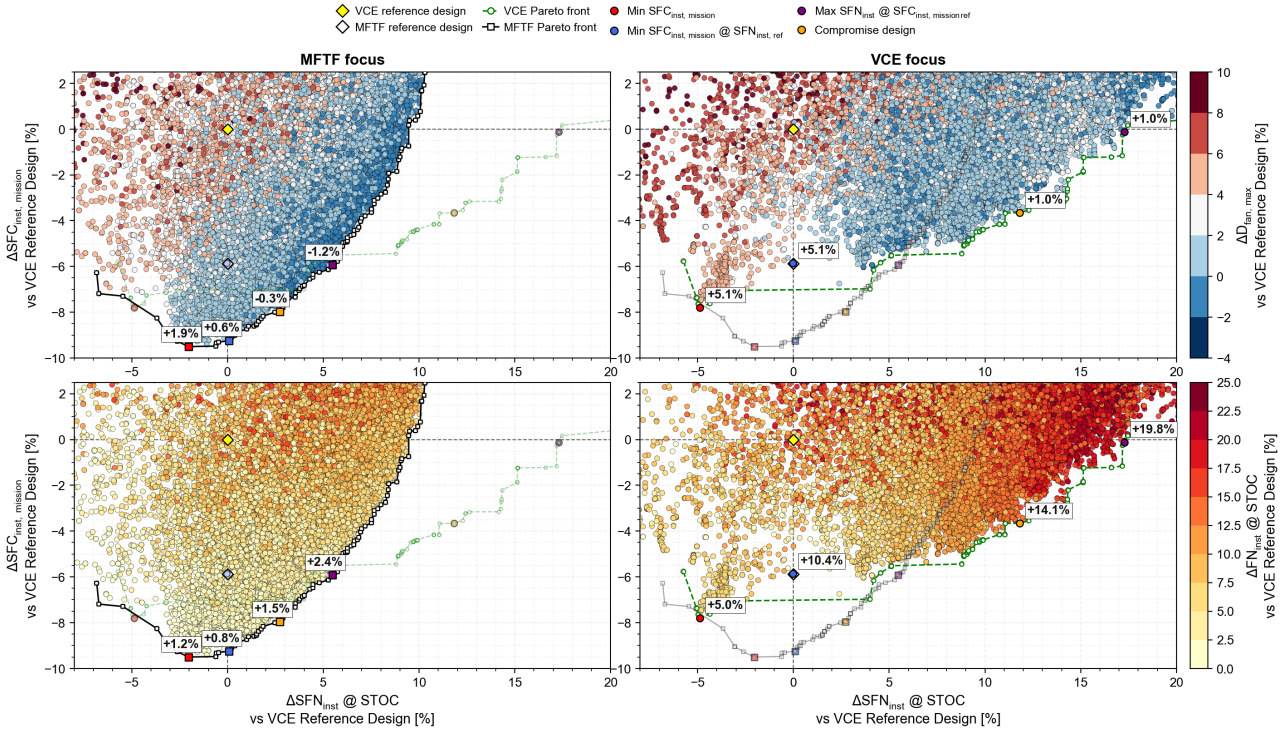


Figure 9 – Architectures' specific feasible design clouds in the objective space evaluated, reported with respect to VCE reference design. Columns are configuration related, while rows present installed specific thrust decomposition

Preliminary weight estimates provide an additional system-level perspective for the comparison between the two configurations. Figure 10 reports the propulsion system weight estimation relative to the VCE baseline configuration, while also indicating the absolute weight of both reference designs. According to the formulation proposed by Torenbeek adopted for the preliminary weight assessment, the reference MFTF results slightly lighter than the VCE. For both architectures, fuel efficient candidates tend to exhibit higher estimated weight, mainly as a consequence of larger engine size and higher OPR levels. For the VCE candidates, uncertainty scenarios of +10%, +20%, and +30 % are included to account for potential weight penalty associated with the increased architectural complexity, variable geometry systems, and third stream implementations.
Nevertheless, VCE architectures may provide potential benefits that are not fully captured either by the optimization objectives or by the preliminary weight estimation. These are mainly related to the installation aspects and aircraft-level integration capabilities. The availability of a third stream surrounding the engine core can introduce an additional degree of freedom related to propulsion-aircraft-thermal management system integration. Acting as a dedicated relatively cold flow path, the third stream can be used for heat rejection purposes, for example in the eventuality of more electrified or hybridized layouts. In such configurations, electrical machine may be integrated in the form of motors, generators, or power transfer enablers (acting as alternative variable geometry features), and additional thermal loads may be introduced in the system.
A further limitation concerns low altitude operation and LTO cycle noise. Since the selected configurations have high specific thrust, low BPR, and high Fan PRs, and despite the introduction of variable

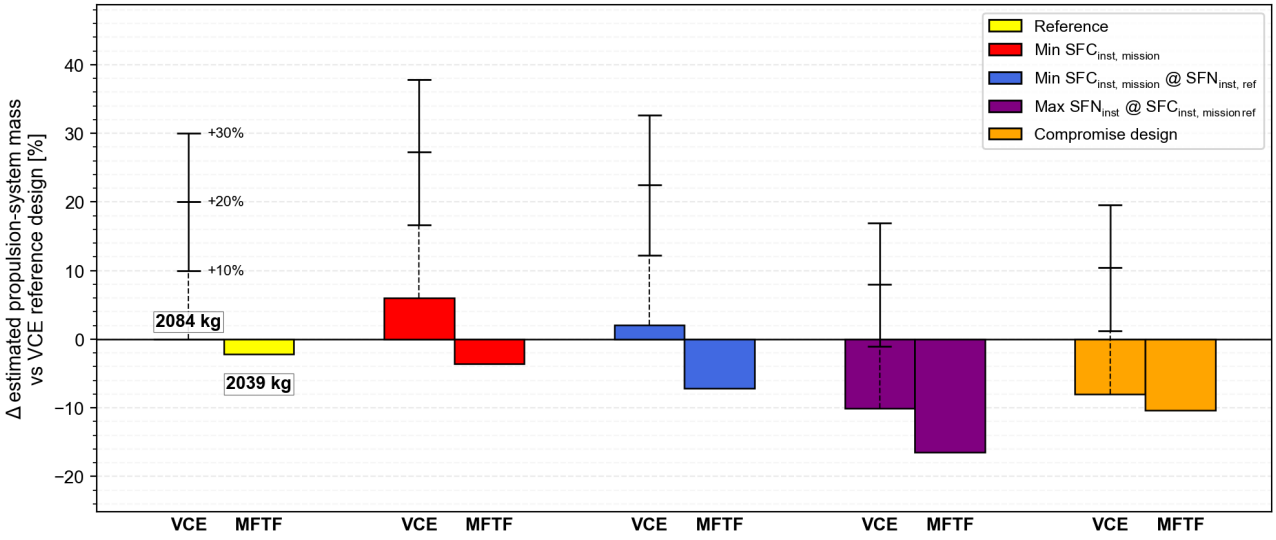


Figure 10 – Preliminary weight estimation using Torenbeek correlation for the reference and selected optimized candidates. For the VCE architecture 3 different uncertainty scenario are included

geometries, achieving subsonic flow conditions at the nozzle results challenging. Previous studies focused on engine architectures shifted towards moderate to high BPRs and low Fan PRs, with variable geometry nozzle, in order to achieve the noise requirement in LTO segments. However this design shift would also lead to a substantial increase in fan diameter and nacelle size, influencing therefore the engine performance during supersonic flight regimes due to installation drag and related effects. Related to this context, the third stream may offer a potential mitigation opportunity. The separate bypass stream could provide acoustic shielding effect, conceptually similar to the bypass stream for high BPR turbofans. However, since the evolving mass flow is expected to be significantly lower, the effectiveness of this mitigation strategy might be limited.
Overall, the comparison indicates that the MFTF architecture provides a robust fuel consumption advantage in the common objective space, with relatively limited architectural complexity and mass uncertainty. The VCE architecture instead offers a broader high specific thrust capability and additional integration potential, especially through the third stream, but these advantages are accompanied by possible penalties in propulsion system mass, mechanical complexity, and LTO noise management. Therefore, the final architecture selection cannot be based only on the two objective Pareto position, but must also account for weight, installation effects, thermal-management requirements, and low-altitude acoustic constraints.

4. Conclusions

This work compared two propulsion system architectures tailored for civil supersonic applications: a Mixed Flow Turbofan and a Variable Cycle Engine. Both configurations were designed using a Multi Point Synthesis approach and assessed through a Multi-Objective Optimization routine, allowing the identification of suitable non-dominated candidates under multiple operating requirements and practical engine constraints.
The results show that the Mixed Flow Turbofan architecture provides a more favourable mission installed specific fuel consumption in the common objective space, while retaining lower architectural complexity and reduced mass uncertainty. For the Mixed Flow Turbofan, reductions in mission installed specific fuel consumption of almost 4% can be achieved at approximately constant installed specific thrust, while the maximum thrust candidate provides an installed specific thrust increase of about 5% at nearly unchanged mission specific fuel consumption. The preliminary mass estimate also indicates a slightly lower reference propulsion system mass for the Mixed Flow Turbofan, compared with the Variable Cycle Engine reference configuration.
The Variable Cycle Engine architecture, instead, extends the feasible design space toward significantly higher installed specific thrust levels, with increments reaching approximately 20% in the se-

lected region of interest. Its main advantage is therefore not necessarily associated with an absolute reduction in mission specific fuel consumption, but rather with the capability to increase thrust density while limiting the corresponding fuel consumption penalty. In addition, the third stream introduces potential integration benefits, especially for future propulsion aircraft thermal-management systems and more electrified engine concepts.
However, these advantages are accompanied by increased mechanical complexity, larger uncertainty in propulsion-system mass, and additional challenges related to low altitude noise management. In the preliminary weight assessment, Variable Cycle Engine uncertainty scenarios of +10%, +20%, and +30% were considered to account for the additional complexity associated with variable geometries and third stream implementation. The selected high specific thrust configurations remain difficult to reconcile with subsonic nozzle flow requirements during Landing and Take-Off operation, even when variable geometry nozzles are considered.

5. Contact Author Email Address

mailto: lorenzo.carrea@mdu.se
Phone number: +46 736620964
Mailing Address: Mälardalen University, Box 883, 721 23 Västerås.

6. Copyright Statement

The authors confirm that they, and/or their company or organization, hold copyright on all of the original material included in this paper. The authors also confirm that they have obtained permission, from the copyright holder of any third party material included in this paper, to publish it as part of their paper. The authors confirm that they give permission, or have obtained permission from the copyright holder of this paper, for the publication and distribution of this paper as part of the ICAS proceedings or as individual off-prints from the proceedings.

7. Acknowledgments

The authors gratefully acknowledge the European Defence Fund (EDF) for the financial support through the NEUMANN (Grant Agreement Number 101103504) project. Funded by the European Union. Views and opinions expressed are however those of the author(s) only and do not necessarily reflect those of the European Union. Neither the European Union nor the granting authority can be held responsible for them.



References

[1] Y. Sun and H. Smith. Review and prospect of supersonic business jet design. *Progress in Aerospace Sciences*, 90:12–38, 2017. DOI: https://doi.org/10.1016/j.paerosci.2016.12.003.

[2] R. Jaron and N. Viola. The future of civil supersonic transport in Europe: the Seneca and More&Less projects. In *Proceedings of the Internationl Congress of the Aeronautical Sciences ICAS 2024*, number ICAS2024-0820, September 9–13 2024. DOI: https://doi.org/10.71945/icas2024_0820.

[3] J. Rathsam, P. Coen, A. Loubeau, L. Ozoroski, and G. Shah. Scope and goals of NASA's Quesst community test campaign with the X-59 aircraft. In *14th ICBEN Congress on Noise as a Public Health Problem*, 2023.

[4] H. R. Welge, J. Bonet, T. Magee, D. Chen, S. Hollowell, A. Kutzmann, A. Mortlock, J. Stengle, C. Nelson, E. Adamson, S. Baughcum, R. T. Britt, G. Miller, and J. Tai. N+2 supersonic concept development and systems integration. Technical Report CR-2010-216842, NASA, August 2010.

[5] SENECA - (LTO) noiSe and EmissioNs of supErsoniC Aircraft. URL: https://seneca-project.eu/.

[6] MORE&LESS - MDO and REgulations for Low-boom and Environmentally Sustainable Supersonic aviation. URL: https://cordis.europa.eu/project/id/101006856.

[7] S. Zenkner, F. Carvalho, R. G. Brakmann, and G. Goinis. Variable cycle engine concepts and component technologies—an overview. *Journal of Engineering for Gas Turbines and Power*, 147(5):051004, 11 2024. DOI: https://doi.org/10.1115/1.4066779.

[8] H. Smith. A review of supersonic business jet design issues. *The Aeronautical Journal*, 111(1126):761–776, 2007. DOI: https://doi.org/10.1017/S0001924000001883.

[9] J. J. Berton, W. J. Haller, P. F. Senick, S. M. Jones, and J. A. Seidel. A comparative propulsion system for the high-speed civil transport. Technical Report TM-2005-213414, NASA, February 2005.

[10] K. Van den Borre and B. H. Saracoglu. Optimization of variable cycle engine throttle schedules using gradient-free methods. *Journal of Engineering for Gas Turbines and Power*, 148(5):051011, 11 2025. DOI: https://doi.org/10.1115/1.4069846.

[11] K. Van den Borre, G. M. Bruno, and B. H. Saracoglu. Quantitative comparison of two variable cycle engine concepts. In *AIAA SCITECH 2026 Forum*, number AIAA2026-0552, January 12–16 2026. DOI: https://doi.org/10.2514/6.2026-0552.

[12] C. Mourouzidis, D. Del Gatto, S. Adamidis, C. Villena Munoz, C. Lawson, B. Martinez Corzo, P. Leyland, D. Marsh, L. Lim, B. Owen, E. Terrenoire, O. Atinault, I. LeGriffon, M. Huet, M. Schaefer, M. Plohr, S. Bake, and P. Madden. Preliminary design of next generation Mach 1.6 supersonic business jets to investigate landing & take-off (LTO) noise and emissions – SENECA. *Journal of Physics: Conference Series*, 2526(1):012011, June 2023. DOI: https://doi.org/10.1088/1742-6596/2526/1/012011.

[13] M. Plohr, S. Zenkner, S. Bake, and D. Zeitz. Thermodynamic design and emissions model of a Mach 1.8 supersonic airliner engine. In *In Proceedings of the Internationl Congress of the Aeronautical Sciences ICAS 2024*, number ICAS2024-0129, September 9–13 2024. DOI: https://doi.org/10.71945/icas2024_0129.

[14] C. Villena Muñoz, C. Lawson, A. Riaz, and A. Sharma. Design of the SENECA Mach 1.8 supersonic airliner with multi-fidelity aerodynamic analysis for noise-optimised Take-Off trajectories. In *Proceedings of the Internationl Congress of the Aeronautical Sciences ICAS 2024*, number ICAS2024-0758, September 9–13 2024. DOI: https://doi.org/10.71945/icas2024_0758.

[15] R. Hutchinson, J. Lawrence, and K. F. Joiner. Conceptual design and integration of a propulsion system for a supersonic transport aircraft. *Proceedings of the Institution of Mechanical Engineers, Part G: Journal of Aerospace Engineering*, 236(3):583–592, 2022. DOI: https://doi.org/10.1177/09544100211016952.

[16] C. Villena Munoz, G. Bonavolontà, C. Lawson, and A. Riaz. Conceptual design of a next generation supersonic airliner for low noise and emissions. In *AIAA SCITECH 2023 Forum*, number AIAA2023-0215, January 23–27 2023. DOI: https://doi.org/10.2514/6.2023-0215.

[17] G. Piccirillo, A. Gregorio, R. Fusaro, D. Ferretto, and N. Viola. Mixed-flow turbofan engine model for the conceptual design of sustainable supersonic airplanes. *Aerospace 2024*, 11(9):740–772, 2024. DOI: https://doi.org/10.3390/aerospace11090740.

[18] G. Piccirillo, N. Viola, R. Fusaro, and L. Federico. Guidelines for the LTO noise assessment of future civil supersonic aircraft in conceptual design. *Aerospace*, 9(27), 2022. DOI: https://doi.org/10.3390/aerospace9010027.

[19] J. J. Berton, D. L. Huff, K. Geiselhart, and J. Seidel. Supersonic technology concept aeroplanes for environmental studies. In *AIAA Scitech 2020 Forum*, number AIAA2020-0263, January 6–10 2020. DOI: https://doi.org/10.2514/6.2020-0263.

[20] T. Schlette and S. Staudacher. Preliminary design and analysis of supersonic business jet engines. *Aerospace 2022*, 9(9):493–516, 09 2022. DOI: https://doi.org/10.3390/aerospace9090493.

[21] K. Deb, A. Pratap, S. Agarwal, and T. Meyarivan. A fast and elitist multiobjective genetic algorithm: Nsga-ii. *IEEE Transactions on Evolutionary Computation*, 6(2):182 – 197, 2002. DOI: https://doi.org/10.1109/4235.996017.

[22] J.S. Schutte. *Simultaneous multi-design point approach to gas turbine on-design cycle analysis for aircraft engines*. PhD thesis, Georgia Institute of Technology, Atlanta, GA, 2009.

[23] M. Sielemann, C. Coic, M. Hubel, X. Zhao, and K. G. Kyprianidis. Introduction to multi-point design strategies for aero engines. In *Proceedings of the ASME Turbo Expo 2020: Turbomachinery Technical Conference and Exposition*, number GT2020-14912, page V006T08A005, September 21–25 2020. DOI: https://doi.org/10.1115/GT2020-14912.

[24] L. Carrea and K. G. Kyprianidis. A multi-objective optimization framework for engine design space exploration in supersonic civil transport applications. In *Proceedings of ASME Turbo Expo 2026: Turbomachinery Technical Conference and Exposition*, number GT2026-178966, June 15–19 2026.

[25] M. Sielemann, M. Thorade, J. Claesson, A. Nguyen, X. Zhao, S. Sahoo, and K. G. Kyprianidis. Modelica and Functional Mock-Up Interface: Open standards for gas turbine simulation. In *Proceedings of the ASME Turbo Expo 2019: Turbomachinery Technical Conference and Exposition*, volume 3, page V003T06A024, June 17–21 2019. DOI: https://doi.org/10.1115/GT2019-91597.

[26] M. Sielemann, A. Pitchaikani, N. Selvan, and M. Sammak. The Jet Propulsion Library: Modeling simulation of aircraft engines. In *Proceedings of the 12th International Modelica Conference*, 2017.

[27] E. J. Kowalski. A computer code for estimating installed performance of aircraft gas turbine engines vol.I - final report. Technical Report CR 159691, NASA, December 1979.

[28] E. J. Kowalski and R. A. Jr Atkins. A computer code for estimating installed performance of aircraft gas turbine engines vol.III - library of inlet/nozzle configurations and performance maps. Technical Report CR 159693, NASA, December 1979.

[29] S. Adamidis, D. Del Gatto, C. Mourouzidis, S. Brown, and V. Pachidis. Installation effects of supersonic inlets on next-generation sst turbofan engines. *Engineering Proceedings*, 90(1), 2025. DOI: https://doi.org/10.3390/engproc2025090050.

[30] W. P. J. Visser. Gas Turbine Engine Simulation at NLR. Technical Report NLR TP 95574 U, National Aerospace Laboratory NLR, Amsterdam, The Netherlands, 1995.

[31] B. Curnock, J. Yin, R. Hales, and P. Pilidis. High-bypass turbofan model using a fan radial-profile performance map. *Aircraft Design*, 4(2-3):115–126, June 2001. DOI: https://doi.org/10.1016/S1369-8869(01)00007-6.

[32] J. Kurzke. Achieving maximum thermal efficiency with the simple gas turbine cycle. Technical report, MTU Aero Engines, 2018.

[33] B. Schneider. Turbine cooling air estimation in thermodynamic simulations. *CEAS Aeronautical Journal*, 16(1):141–156, January 2025. DOI: https://doi.org/10.1007/s13272-024-00776-0.

[34] J. Kurzke, I. Halliwel, and R. Hill. *Propulsion and Power: An Exploration of Gas Turbine Performance Modeling*. Springer International Publishing AG, 2nd edition, 2025. ISBN: 978-3-031-65025-3.

[35] L. Carrea, K. G. Kyprianidis, and J. Claesson. Elements of cycle design for parallel hybrid mixed flow turbofans: select trade-offs in performance and energy efficiency. In *Proceedings of the 12th Swedish Aerospace Technology Congress*, number FT2025-88822, October 14–15 2025. DOI: https://doi.org/10.3384/wcc215.1154.

[36] K. G. Kyprianidis and E. Dahlquist. On the trade-off between aviation NOx and energy efficiency. *Applied Energy*, 185:1506–1516, 2017. DOI: https://doi.org/10.1016/j.apenergy.2015.12.055.

[37] P. Lolis, P. Giannakakis, V. Sethi, A. J. B. Jackson, and P. Pilidis. Evaluation of aero gas turbine preliminary weight estimation methods. *The Aeronautical Journal*, 118(1204):625–641, 2014. DOI: https://doi.org/10.1017/S0001924000009404.

[38] Kuz´michev, V., Krupenich, I., Filinov, E., and Ostapyuk, Y. Comparative analysis of mathematical models for turbofan engine weight estimation. *MATEC Web Conf.*, 220:03012, 2018. DOI: https://doi.org/10.1051/matecconf/201822003012.

[39] K. G. Kyprianidis. *On Gas Turbine Conceptual Design*. PhD thesis, Cranfield University, School of Aerospace, Transport and Manufacturing, 2019.

[40] M. Sielemann, C. Coïc, X. Zhao, D. E. Diamantidou, and K. G. Kyprianidis. Multi-point design of parallel hybrid aero engines. In *AIAA Propulsion and Energy 2020 Forum*, number AIAA2020-3556, August 24–28 2020. DOI: https://doi.org/10.2514/6.2020-3556.

[41] J. S. Schutte, J. Tai, J. Sands, and D. Mavris. Cycle design exploration using multi-design point approach. In *Proceedings of the ASME Turbo Expo 2012: Turbine Technical Conference and Exposition. Volume 1: Aircraft Engine; Ceramics; Coal, Biomass and Alternative Fuels; Controls, Diagnostics and Instrumentation*, Turbo Expo, pages 271–281, 06 2012. DOI: https://doi.org/10.1115/GT2012-69334.

[42] H. I. H. Saravanamuttoo, G.F.C Rogers, H. Cohen, P.V. Straznicky, and A.C. Nix. *Gas turbine theory*. Pearson, Harlow, England, 7th edition, 2017. ISBN: 978-1-292-09309-3 1-292-09309-9.

[43] H. Smith and Y. Sun. Design Case of the E-19 AEOLUS Supersonic Business Jet. In *AIAA Aviation Forum 2020*, number AIAA2020-2618, June 15–19 2020.

[44] D. Del Gatto, S. Adamidis, C. Mourouzidis, and S. Brown. Comparison of alternative engine architectures for next generation supersonic aircraft. *Engineering Proceedings*, 90(1), 2025. DOI: https://doi.org/10.3390/engproc2025090115.

[45] J. D. Mattingly, W. H. Heiser, K. M. Boyer, B. A. Haven, and David T. Pratt. *Aircraft Engine Design*. AIAA Education Series. AIAA - American Institute of Aeronautics and Astronautics, Reston, VA, 3rd edition, 2018. ISBN: 978-1-62410-517-3.

[46] K. G. Kyprianidis. *Future Aero Engine Designs: An Evolving Vision*, pages 3–24. InTech, 11 2011. ISBN: 978-953-307-611-9, DOI: https://doi.org/10.5772/19689.